Chapter 3

Yb:YAG-Pumped, Few-Cycle Optical Parametric Amplifiers

Hanieh Fattahi

Additional information is available at the end of the chapter

http://dx.doi.org/10.5772/64438

Abstract

In this chapter, the principle, design, and characteristics of high-efficiency, short-pulse-pumped, few-cycle optical parametric chirped-pulse amplification (OPCPA) systems are reviewed. To this end, the feasibility of two techniques to increase the conversion efficiency of few-cycle OPCPA systems is demonstrated and discussed. The techniques result in 2.5 mJ, 7.5 W pulses and correspond to a pump-to-signal conversion efficiency of 30%. The broadband amplified spectrum supports 5.7 fs. Finally, the feasibility of extending the amplified spectrum to a near-single-cycle regime by using the combination of different crystals and phase matching is shown.

Keywords: optical parametric chirped-pulse amplification, Yb:YAG thin-disk laser, attosecond pulse, femtosecond laser

1. Introduction

The new generation of femtosecond technology based on short-pulse-pumped optical parametric chirped-pulse amplification (OPCPA) [1] holds promise for scaling the peak power and average power of few-cycle pulses simultaneously. This progress would benefit a number of fields, notably attosecond science [2, 3] by allowing to scale attosecond pulse generation at higher photon energy and higher flux.

In OPCPA, the amplified bandwidth is not limited by the energy level structure of a laser medium or gain narrowing [4], as is the case in laser amplifiers [5]. Therefore, OPCPA appears to be the method of choice for the production of ultrashort pulses (down to the few-cycle regime) at high peak and average power. Employing short pulses (several-ps to sub-ps) to

pump an OPCPA allows higher peak intensity in the nonlinear medium as the damage threshold intensity of materials scales with the inverse square root of the pulse duration [6]. The high pump intensity makes it possible to achieve the required gain in a shorter crystal, which leads to greater amplification bandwidth.

Further advantage with a short crystal is that the effect of transverse walk-off is reduced, the temporal contrast can be enhanced, and stretchers and compressors can be simpler. However, the crystal length does not decrease as rapidly as the pulse duration, so the temporal walk-off relative to the pulse duration increases for short pulses. A simple analytical analysis shows that the optimum pump-pulse duration to achieve a high conversion efficiency and a broadband gain is around 1 ps [7].

Nevertheless, all these advantages of short-pulse-pumped OPCPA remain useless without an efficient, reliable, and powerful pump source. Such pump lasers are required to deliver high-energy near-1-ps pulses with near-diffraction-limited beam quality at repetition rates in the kHz to MHz range.

Heretofore, due to the lack of suitable pump lasers, the few-cycle OPCPA delivered either high-energy pulses at a low repetition rate [8, 9] or low-energy pulses at a high repetition rate [10]. Nowadays, Yb-doped lasers in the thin-disk, fiber or slab geometries [1, 11–15] are capable of delivering high-energy, high average power pulses with ps-pulse duration. Among these laser technologies, the recent advances in Yb:YAG thin-disk lasers have started to fulfill the criteria for suitable pump sources for OPCPA systems and hold promise to change the current state of the art of OPCPA systems to few-cycle pulses with higher energy and average power [1, 16].

This chapter is devoted to the recent progress in Yb:YAG-pumped, few-cycle OPCPA systems. In Section 1, a brief overview on the fundamentals of OPCPA is presented. In Sections 2 and 3, novel techniques for increasing the conversion efficiency are discussed. In Section 4, a technique for extension of the amplification bandwidth is discussed.

In a medium with second-order nonlinearity, a high-energy photon (called pump) can decay to two newly generated photons with lower frequencies (called seed and idler). In the presence of initial seed photons, the decay of pump photons is stimulated and consequently more photons at the seed frequency are generated. The seed photons after amplification are named signal and the process is called optical parametric amplification (OPA). The frequency of the generated signal and idler photons is defined by the conservation of energy. However, the amplification bandwidth can be increased by fulfilling conservation of momentum between pump, signal, and idler pulses, which can be tuned by the type, thickness, and temperature of the nonlinear medium and also the geometry of the three interacting beams.

To obtain a strong pump-to-signal and idler energy conversion, the spatial and temporal overlap between seed and pump pulses in the nonlinear medium should be maximized. The optimum temporal overlap between the pump and seed pulses can be ensured by temporal stretching of the seed pulses to the temporal window of pump pulses. This technique is the combination of chirped-pulse amplification (CPA) [17] and OPA, hence called optical parametric chirped-pulse amplification.

http://dx.doi.org/10.5772/64438

In addition to the above-mentioned parameters, the conversion efficiency in OPA or OPCPA systems also depends on the thickness of the nonlinear medium, peak intensity of the pump pulses, and the initial seed energy. Conversion efficiency scales up by increasing the thickness of the nonlinear medium as long as the phase-matching condition (conservation of momentum) between the three interacting beams is satisfied. At higher pump peak intensity to induced nonlinear polarization in the nonlinear medium is stronger and therefore larger amplification is achieved. Moreover, by increasing the seed-to-pump energy ratio, the conversion efficiency at lower amplification gain can be achieved.

The optimization of the pump-to-signal conversion efficiency of multicycle OPCPA systems has been the subject of several studies [18–22]. In the next two sections, the feasibility and realizability of two techniques to increase the conversion efficiency of few-cycle OPCPA systems are discussed.

2. Recycling the pump energy

In optical parametric amplification, the behavior of the gain over the length of the nonlinear medium can be divided into three main regions (**Figure 1(a)**). In the beginning, the energy of the amplified signal has an exponential growth due to the generation of the idler field that enhances the amplification process (region A). In region B, the gain drops gradually as the pump energy is reduced, and the growth of the signal power becomes approximately linear. When the pump beam has been locally depleted at some point in time and space, back conversion sets in and further reduces the gain. In region C, back conversion dominates, and the signal power drops. In the case of pulses with Gaussian spatiotemporal profile, the depletion mainly occurs at the center of the pulse, where the intensity is highest. Therefore, the back conversion already starts before the complete depletion of the pump. Because back conversion depends on both signal and idler beams, it can be reduced by removing the idler between the stages of a multistage OPCPA.

To explore this option, three different designs (as shown in **Figure 1(b)**) are simulated and compared using the SISYFOS code [23]. In all designs, the amplification takes place in a type-I BBO crystal, where the angle between the Optical axis and the signal is 22°, and the noncollinear angle between the pump and the signal in the tangential phase-matching geometry is 2.7°. The pump have a Gaussian beam and pulse shape, and the seed have the Gaussian beam shape and a super-Gaussian spectrum of order 4, ranging from 600 to 1100 nm and linearly chirped to 1.1 ps pulse duration. Higher-order nonlinear effects and parasitic processes were not taken into account.

Figure 1(c) compares the three simulated OPCPA systems. The first configuration (Design 1 in **Figure 1(b)**) consists of a single OPCPA stage using a 2 mm thick BBO crystal, with 7 mJ of pump energy at a peak intensity of 80 GW/cm^2, which results in a conversion efficiency of 14%.

The second design (Design 2 in **Figure 1(b)**) has two stages, and the idler beam is removed between the two stages. This reduces back conversion in the second stage and allows operation

in a regime with stronger pump depletion. Temporal and spatial overlap of the beams could be readjusted between the stages, and a further advantage with the two-stage design is that the phase-matching of the crystals can be tuned slightly differently to optimize the total bandwidth. The crystal lengths for the two stages are 1.2 and 0.7 mm, respectively. The second stage is pumped by the residual pump energy from the first stage resulting in a conversion efficiency of 34%.

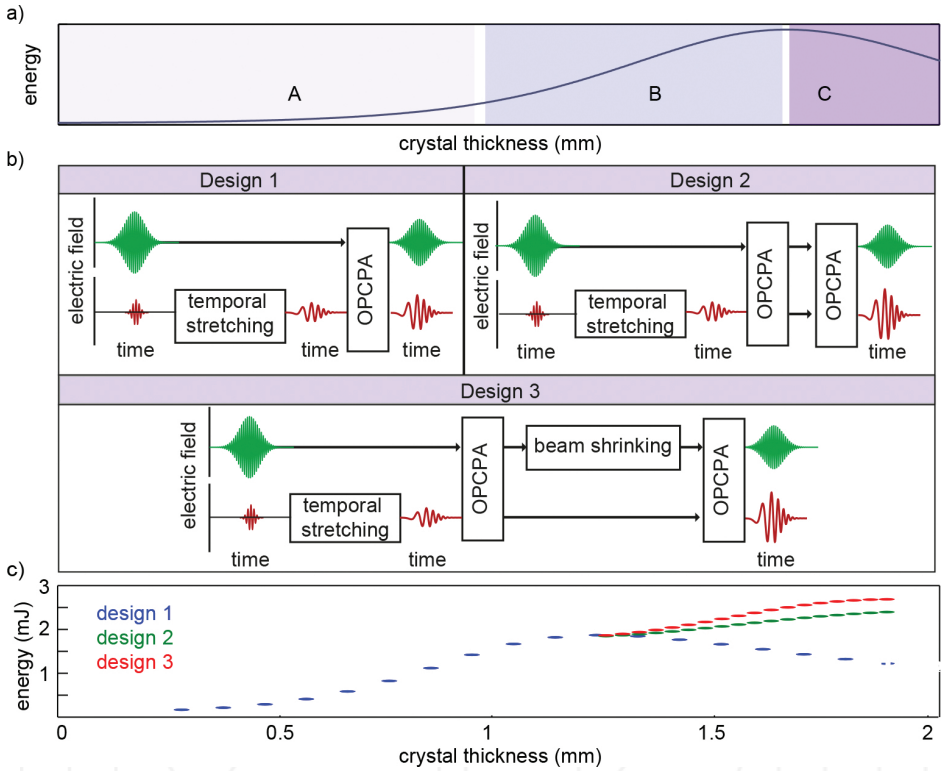

Figure 1. (a) Qualitative behavior of OPCPA amplified energy over the length of the nonlinear medium. (b) Three OPCPA designs are discussed in the main text. Design 1 consists of one OPCPA stage. Designs 2 and 3 consist of two OPCPA stages, where the residual pump energy after the first OPCPA stage is reused in the second stage. In Design 3, the pump after the first amplification stage is resized to increase the pump peak intensity. (c) Calculated amplified signal energy over the crystal length for the three different designs.

The third configuration (Design 3 in **Figure 1(b)**) is a two-stage OPCPA system similar to the second design except that the pump-beam size between the two stages is reduced to compensate the reduction in the pump intensity after the first stage of amplification and therefore the efficiency in the third design reaches 39%.

All three designs are capable of supporting the ultrabroad amplification bandwidth necessary for a few-cycle pulse durations. The detailed parameters of the simulations are shown in

Table 1. In what follows, the experimental realization of the third design is demonstrated and discussed. The third design is chosen as it supports the highest conversion efficiency in the above-mentioned study.

	Design 1	**Design 2**		**Design 3**	
	1st stage	**1st stage**	**2nd stage**	**1st stage**	**2nd stage**
L (mm)	2	1.2	0.7	1.2	0.7
E amp (mJ)	1	1.8	2.4	1.8	2.7
ϕ_p (mm)	2.5	2.5	–	2.5	2
ϕ_s (mm)	2.5	2.5	–	2.5	D^*_{amp}
Efficiency (%)	14	26	14	26	21
Overall efficiency (%)	14	34		39	

D^*_{amp}: the diameter of the amplified beam.

Table 1. Parameters used in simulations: L_c, crystal thickness; $E_{s\,\text{amp}}$, amplified signal energy; ϕ_p, pump-beam diameter at full width at half maximum; ϕ_s, seed beam diameter at FWHM.

2.1. System description

2.1.1. Front end

The experimental OPCPA setup (as shown in **Figure 2**) consists of a Ti:Sa-based oscillator and amplifier followed by a broadband nonlinear seed generation scheme, a pump laser, a temporal jitter compensation system, three OPCPA stages, and a chirped-mirror compressor [24]. The Yb:YAG regenerative amplifier [25], optically synchronized with the OPCPA seed [26], delivers 16 mJ, 1.6 ps pulses at full width at half maximum (FWHM) at 3 kHz repetition rate and its frequency doubled output is used for pumping the OPCPA. However, due to the long optical beam-path difference between seed and pump pulses, timing fluctuations occur due to air turbulence, mechanical vibrations of optical components, temperature drifts, and the finite stability of the front end, which need to be compensated by an active stabilization system. The timing jitter in our system is reduced to a level of 24 fs (root mean square) by using an active stabilization system based on spectrally resolved cross-correlation between the stretched seed and the pump pulse [27].

The broadband OPCPA seed was generated by using a small portion of the output of the Ti:Sa multipass amplifier (Femtolasers GmbH), providing a spectral bandwidth of 60 nm (FWHM) centered at 790 nm. These pulses, containing 30 μJ of energy, focused on a 15 cm long hollow core fiber (HCF) with an inner diameter of 120 μm filled with 4.5 bar of krypton. The pressure of krypton in the HCF and the group delay dispersion (GDD) of the input pulse were optimized to obtain the maximum spectral broadening, covering a spectral range from 500 to 1050 nm.

With this combination of parameters, an overall throughput of 10 μJ pulse energy in a near-diffraction-limited output beam containing the broad spectrum was achieved (**Figure 3(a)**).

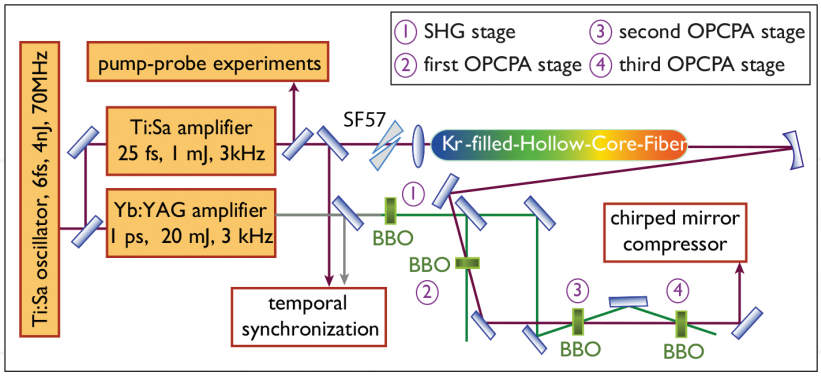

Figure 2. Block diagram of the OPCPA system. The OPCPA broadband seed pulses are generated from a Ti:Sa regenerative amplifier. The output of a Yb:YAG thin-disk amplifier, after frequency doubling, is used to pump the three OPCPA stages. Finally, a chirped-mirror compressor is used for pulse compression of the broadband amplified pulses.

In order to measure the amount of introduced material dispersion, which needs to be compensated after the final OPCPA stage, the broadband seed was sent through the entire beam path without any pump. Pulse dispersion was caused over merely 5.5 mm beam path in BBO, 4 mm path length in SF57 glass, and over 10 m propagation in air. The stretched seed pulses were characterized by a multishot, second harmonic generation (SHG)-XFROG device incorporating a 20 μm thick BBO crystal cut at 29° as the nonlinear medium, while a fraction of the multipass amplifier's output provided the reference beam. From these measurements, a second-order spectral phase of 1433 fs^2 evaluated at 850 nm was retrieved. This is in excellent agreement with the GDD introduced by the above components, evaluated as 1403 fs^2. The pulse duration of the seed pulses assuming a Gaussian fit for the retrieved time structure is 1.1 ps (FWHM), which ensures a sufficiently good temporal matching between the seed and pump pulses in the OPA stages.

For frequency doubling of the pump laser, a BBO crystal was used. Its high nonlinearity allowed the use of a relatively short crystal keeping the accumulated B-integral in the system negligible. Using a BBO crystal of 1.5 mm length, a conversion efficiency as high as 70% with a good beam quality was obtained. The high SHG efficiency confirms the excellent beam quality and clean output pulses of the regenerative amplifier. However, in order to definitely avoid problems related to the B-integral in the OPCPA stages, a 1 mm BBO crystal for the SHG was chosen, which resulted in a conversion efficiency of 57%.

2.1.2. OPCPA stages and pulse compression

The OPCPA setup consists of three stages. We added an OPCPA-based preamplifier stage in the experiment in order to boost the seed energy before the two power amplifier stages. This

http://dx.doi.org/10.5772/64438

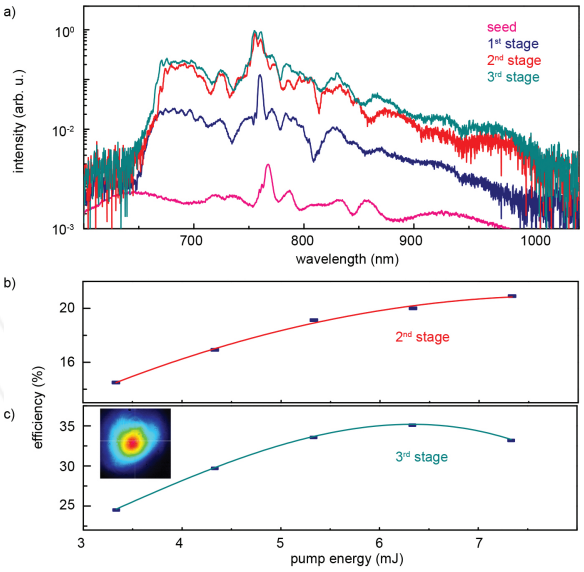

d)

	L_c(mm)	E_{pump}(mJ)	E_{signal}(mJ)	efficiency
1st stage	1.5	1	0.12	12 %
2ndstage	2	7.3	1.7	20.5 %
3rd stage	2	–	2.5	30.1 %

Figure 3. (a) The seed spectrum and the amplified spectra of three OPCPA stages, normalized to the output energy of each stage. (b) and (c) Conversion efficiencies after the second and third stages, respectively. The conversion efficiency is defined as the net increase in signal energy divided by the input pump energy of stage two. (d) The detailed parameters of each OPCPA stage. The total efficiency after each stage is defined as the net increase in signal energy after the stage divided by the total pump energy of the OPCPA chain. Inset: amplified beam profile after the third stage [7].

stage is necessary to drive the following stages into saturation [7]. Therefore, 1 mJ of the frequency doubled output of the thin-disk amplifier was used to pump a 1.5 mm BBO crystal, and an amplified energy of 120 μJ and a 350 nm broad spectrum were achieved in the first stage (**Figure 3(a)**). Here, the OPCPA crystal length was chosen to minimize the superfluorescence at the third stage [28].

The following two stages were designed for reaching the highest possible pump-to-signal conversion efficiency by controlling the idler energy and recycling the pump energy. Up to 7.3 mJ of the pump energy with the peak intensity of 80 GW/cm^2 at 515 nm was used for the second OPCPA stage that employed a 2 mm thick BBO crystal. In this stage, an amplified pulse energy of 1.77 mJ was obtained. The thickness of the crystal at this stage is adjusted to stop amplification slightly below the saturation while preserving a good residual pump-beam quality.

Subsequently, the size of the remaining pump beam was reduced to increase the peak intensity to 80 GW/cm^2 in the third amplification stage. Here, by employing a 2 mm thick BBO crystal, the amplified energy reached 2.5 mJ. In the last two OPCPA stages, an optical-to-optical

conversion efficiency of >32% was achieved (**Figure 3(b)** and **(c)**), which to the best of our knowledge is the highest reported conversion efficiency for few-cycle OPCPA systems [9, 10, 29, 30]. No measurable superfluorescence background was observed when blocking the signal beam in front of the first stage.

The simulated boost efficiency in our design study is in good agreement with the experimental results. Quantitative comparison shows, however, that higher conversion efficiencies were yielded for a shorter crystal in the simulation than in the experiment. We relate the deviation from the theoretical prediction to a slight ellipticity in our pump beam, caused by the compressor of the Yb:YAG amplifier, which limited the effective interaction area between pump and signal beams.

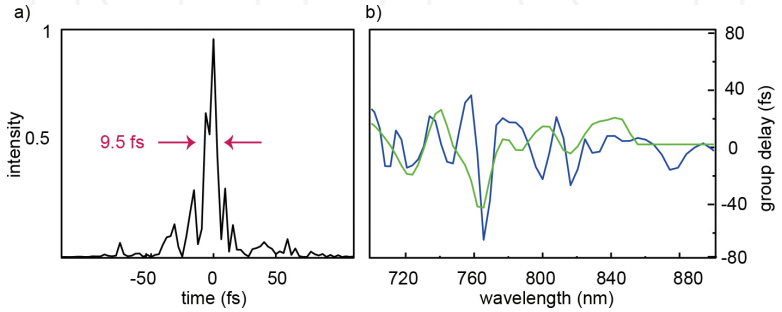

Figure 4. (a) Retrieved temporal intensity of the compressed pulses after 12 reflections in a double-angle chirped-mirror compressor measured by SH-FROG. The pulse is compressed to 9.5 fs and holds Fourier transform limit of 5.7 fs. (c) The calculated GD of retrieved spectral phase for the pumped (blue curve) and unpumped (green curve) OPCPA chains.

The 350 nm broad amplified signal measured with the Si-based spectrometer supports a transform-limited pulse duration of 5.7 fs. Preliminary compression, by using 12 reflections on double-angle chirped mirrors with −30 fs^2 GDD per reflection, resulted in a pulse duration of 9.5 fs (FWHM). The compressor had a total throughput of 80%. The retrieved temporal intensity profile and retrieved residual group delay (GD) of the pulses are shown in **Figure 4(a)** and **(b)**. Our analytical study shows that the pulse can be compressed to 7 fs by adding the GD of a 0.5 mm thick fused silica to the measured GD of the pulse. However, to investigate the origin of the fine oscillation in the retrieved GD, a frequency resolved optical gating (FROG) measurement of the whole OPCPA chain was performed, but this time without any pumping. The comparison between two cases in **Figure 4(b)** shows that oscillations were enhanced by amplification but did not originate from the OPCPA phase [31]. The peak of the GD is at 760 nm, which coincides with the wavelength of Ti:Sa amplifier's pulses and the peak in the spectral intensity of the seed pulses after the HCF. Therefore, it can be concluded that the measured residual higher-order chirp is due to the self-phase modulation in the HCF, OPCPA phase, and the residual oscillations in group delay dispersion of the double-angle chirped-mirror compressor [32, 33]. The higher-order dispersion and the satellite pulses can be compensated

by using specially designed chirped mirrors for this system along with the implementation of spectral smoothing techniques, such as cross-polarized wave generation [34] after the HCF.

The demonstrated highly efficient compact OPCPA system delivers broadband pulses with 2.5 mJ energy supporting a two-cycle pulse at a repetition rate of 3 kHz. Our simple OPCPA design shows that, by extraction of the idler energy and optimization of the pump peak intensity, a higher conversion efficiency can be achieved. The output of the system ensures to be compressible to its two-cycle transform limit by using specially designed chirped mirrors. The system also has the capability to operate with a stabilized carrier envelope phase (CEP) by stabilizing the Ti:Sa oscillator. These features make the reported OPCPA system a suitable driver for high harmonic generation (HHG) [35].

In the next section, an alternative method to achieve high conversion efficiency as well as uniform amplified spectrum is discussed.

3. Controlling the deposition of pump energy

In this section, the realizability of a second novel technique that allows the simultaneous increase in the spectral bandwidth and optical conversion efficiency of OPCPA systems is discussed. This approach is based on a patent application by Deng and Krausz [36].

In the conventional OPCPA systems, similar to the one described in Section 2, the seed-pulse duration is designed to be a fraction of pump-pulse duration in order to maximize the energy conversion. Here as the seeds are strongly chirped, the temporal intensity profile of the pump pulses has to be nearly constant to ensure uniform amplification for the entire seed spectrum. Therefore, for pump pulses with Gaussian temporal profile, the seed pulses have to be considerably shorter than the pump pulses. Consequently, the pump energy is not consumed efficiently and the relative seed-to-pump pulse duration ratio will be a compromise between the amplification bandwidth and the conversion efficiency.

These deficiencies can be overcome if OPCPA seed pulses are linearly stretched to several times longer than the pump pulses. Subsequently, different fraction of seed pulses can be temporally overlapped with pump pulses and are amplified in different OPCPA stages.

This technique enables the controlled deposition of pump energy in the subsequent temporal/spectral locations along the chirped seed pulse [36]. Furthermore, by controlling the amplification gain in each stage, the spatiotemporal profile of the pump pulses can be shaped into a flat-top pulse. By tuning the phase-matching angle of the crystal to the central wavelength of the seed pulse, the ultimate amplified spectrum can be shaped and a broader amplified bandwidth is gained. In addition, by reusing the pump energy after each amplification stage, the total conversion efficiency is increased.

3.1. Theoretical analysis

Figure 5 shows simulation results for three different OPCPA designs. The simulation's input parameters are similar to the ones presented in Section 2.

In the first design, the residual pump energy after the first amplification stage is used to pump the second stage and ultimately the residual pump energy after the second stage is used to pump the third stage.

Due to the Gaussian shape of the pump in time and space, the energy extraction takes place primarily in the middle of the pump. Therefore, the wings are mostly left unaffected with a signature of energy back conversion at the center, due to the fact that this part of the pump possesses the highest peak intensity. In this design, the OPCPA pump-to-signal conversion efficiency is increased to 43% compared to the OPCPA system demonstrated in Section 2 (**Figure 5(b)** and **(c)**).

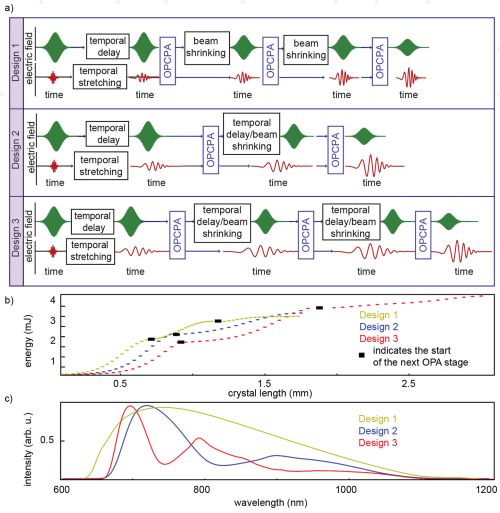

Figure 5. (a) Three designs are discussed in the main text. Design 1 consists of three OPCPA stages, where the residual pump energy after each amplification stage is reused in a subsequent OPCPA stage. Design 2 consists of two OPCPA stages. Here, the seed pulses are temporally stretched to twice the pump-pulse duration, and the residual pump energy after the first OPCPA stage is reused in the second stage. In Design 3, the seed pulses are temporally stretched to triple of the pump-pulse duration, and the residual of the pump energy is reused after each amplification stage. (b) Calculated amplified signal energy over the crystal length and their corresponding spectra (c) for the three different designs [7].

In the second design, the seed pulses are stretched temporally to twice the pump-pulse duration. The blue part of the seed spectrum is amplified in the first OPCPA stage by adjusting the temporal overlap between pump and seed pulses. Subsequently, the pump pulses after the first stage are reused to amplify the red part of the spectrum at the second stage. In this design, the pump-to-signal conversion efficiency reaches 45% indicating the good pump-energy extraction while the beam quality of the amplified signal is maintained (**Figure 5(b)** and **(c)**).

The 45% conversion efficiency achievable from the second design is not drastically different from the 38.6% efficiency achievable from the case where the seed and pump pulses have the

http://dx.doi.org/10.5772/64438

same pulse duration (as discussed in Section 2) as the pump pulses after the first amplification stage in both cases maintain a good spatiotemporal profile.

The gain and the shape of the amplified spectrum can be further optimized by adjusting the phase-matching angles of the crystal in each stage to tune the amplification for the selected part of the spectrum, which is not investigated in this study.

In the third design, the seed pulses are stretched three times the pump pulses and amplified in three subsequent OPCPA stages, while the residual pump energy of the preceding stage is used to pump the subsequent stage. The bluest frequencies of the seed spectrum are amplified in the first stage, while the reddest frequency components are amplified in the third OPCPA stage. The pump-to-signal conversion efficiency in this design reaches 57%, which is a noticeably higher value compared to the other designs (**Figure 5(b)** and **(c)**). The spectral narrowing for Designs 2 and 3 is caused by a suboptimal stretching factor of the input signal and phase-matching angle of the crystal. The optimizations of these parameters are cumbersome in simulation but straightforward in an experimental setup.

3.2. Experimental setup

The seed pulses of the OPCPA system described in Section 2 are stretched after the first amplification stage by using an 8 mm thick SF57 plate at Brewster's angle. The blue frequencies of the seed spectrum were amplified to 4 W by adjusting the temporal delay between the seed and pump pulses and adjusting the phase-matching angles of the BBO crystal (blue curve in **Figure 6(a)**). In the next OPCPA stage, the amplification is moved to the second half of the seed spectrum gaining 6 W of the total amplification (**Figure 6(a)**, pink curve).

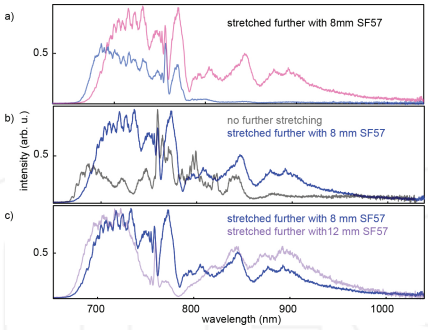

Figure 6. (a) The experimental demonstration of Design 2. The seed pulses are heavily stretched by using an 8 mm thick SF57 plate. The higher frequencies in the spectrum are amplified first (blue curve). The residual of the pump energy is used to amplify the lower frequency components of the spectrum (pink curve). (b) The gray curve shows the amplified spectrum in the similar OPCPA system without any spectral stacking (gray curve) compared to the amplified spectrum shown in (a) (blue curve). (c) Further stretching of the seed pulses by using a 12 mm thick SF57 plate results in appearing of a hole in the amplified spectrum (purple curve) [7].

The same setup, after removing the bulk stretcher, resulted in 6.2 W of amplification after the third stage. As shown in **Figure 6(b)**, the amplified spectrum of the stacked OPCPA is more

uniform due to the even amplification gain. The red wing of the spectrum carries more energy in the stacked OPCPA compared to the amplified spectrum achieved from the system discussed in Section 2. Moreover, the spectral spike at 780 nm is heavily suppressed. **Figure 6(c)** shows amplified spectrum for a similar system but with a larger stretching factor. Here, after stretching the seed pulses using a 12 mm thick SF57 plate, 5 W of the average power was obtained. It can be seen that the amplified spectrum contains a hole, leaving the 8 mm thick SF57 plate, the optimum thickness for temporal stretching of the seed pulses.

Temporal stretching of the signal pulses to twice the pump-pulse duration, demonstrated in this section experimentally, did not show further increase in the OPCPA conversion efficiency compared to the scheme realized in Section 2. This similarity in the conversion efficiency is due to the fact that the spatiotemporal quality of the residual pump pulses after one amplification stage is preserved for both cases.

However, it is shown analytically that the further temporal stretching of seed pulses results in the increase in the conversion efficiency, as the spatiotemporal quality of the remaining pump pulses after two amplification stages is preserved just for the case of heavily chirped input seed.

4. Gain bandwidth engineering

The bandwidth of the amplified spectra, as discussed in the previous sections, can be extended further by using different crystals or a crystal with different phase-matching angles. The combination of BBO and LiB_3O_5 (LBO) crystals can be used to extend the amplified spectrum to longer frequencies, as the BBO crystal does not support amplification for spectral components above 1.1 μm. The amplified spectrum in both crystals supports near-single-cycle pulses, which is not unobtainable with solely either of them.

To this end, the broadened seed spectrum generated in the HCF subsequently focused on a 4 mm $Y_3Al_5O_{12}$ (YAG) crystal to extend the spectrum to 1400 nm and is amplified in an OPCPA chain similar to the system described in Section 2. Combinations of LBO and BBO crystals at different OPCPA stages are used to increase the amplification bandwidth. The first OPCPA stage was optimized to amplify a broad spectral range from 750 to 1400 nm up to 50 μJ energy in a 2 mm LBO crystal. In the second stage, a 2 mm BBO crystal was employed. The amplified spectrum measured in this stage, using an Si-based spectrometer, spans from 670 to 1100 nm and contained 1.1 mJ energy. Finally at the third stage, 1.8 mJ energy was obtained in a 3 mm LBO crystal.

The amplified spectra at each OPCPA stage, normalized to their energy, are shown in **Figure 7**. The amplified spectrum obtained after the third stage supports 4.3 fs transform-limited pulses (FWHM). The preliminary pulse compression was performed by using a set of chirped-mirror compressor designed for spectral wavelength of 700–1300 nm. **Figure 7(b)** shows the pulse compression to 9 fs measured with an SH-FROG containing a 10 μm BBO crystal. The retrieved spectrum from the FROG measurement is in a good agreement with a

spectrum measured after the third OPCPA stage. Pulse compression to its Fourier transform limit would require a specially designed chirped-mirror compressor for compensating the higher-order chirp.

The conversion efficiency of the system can be optimized further by using a longer crystal in the last OPCPA stage without relinquishing the amplified spectral bandwidth.

As shown in this section, the utilization of different well-selected nonlinear crystals extends the OPCPA gain bandwidth substantially. The realized three-stage OPCPA system, using one BBO and two LBO crystals, delivers 1.8 mJ pulses with a Fourier transform limit of 4.5 fs. The system supports shorter pulse duration than an all-LBO three-stage OPCPA system with 5.3 fs (FWHM) pulses. The reported extension of the amplified spectral bandwidth is crucial for experiments that rely on high-energy, single-cycle pulses.

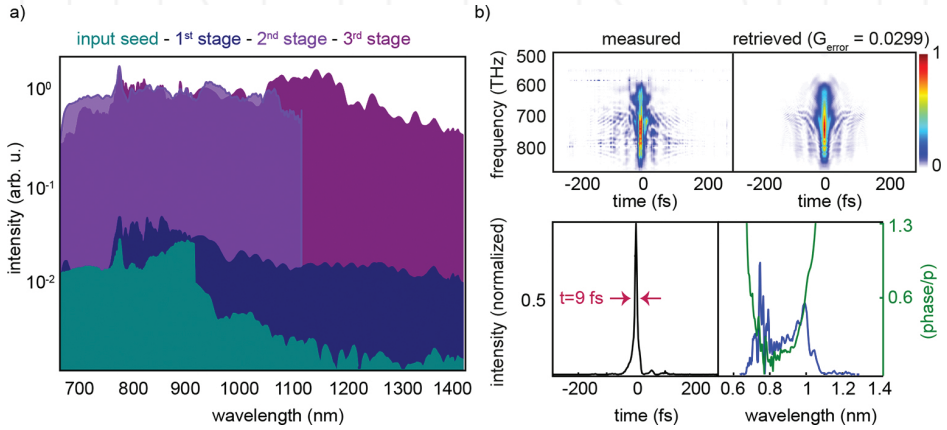

Figure 7. (a) Amplified spectra in a three-stage OPCPA system. A 2 mm LBO crystal is used to amplify the spectral components from 750 to 1400 nm in the first OPCPA stage. In the second stage, the spectral components from 680 to 1100 nm were amplified in a 2 mm BBO crystal and finally in the last stage a 3 mm LBO crystal is used to boost the amplification to 1.8 mJ. (b) Measured and retrieved SH-FROG traces (top) and the retrieved spectrum and temporal profile of the pulses (bottom) of the OPCPA system [7].

5. Summary

In this chapter, three few-cycle OPCPA systems operating at the near-infrared spectral range and pumped by the second harmonic generation of a Yb:YAG thin-disk amplifier were reviewed. The feasibility of increasing the conversion efficiency of the system by reusing the pump energy after each amplification stage, in the subsequent OPCPA stages, was demonstrated. It was shown that by controlled deposition of pump energy in different parts of the seed spectrum, high conversion efficiency along with a smooth amplified spectrum can be achieved. Furthermore, the feasibility of TW-level monocycle OPCPA systems was studied by

using different crystals in different amplification stages. In addition to the presented systems, different harmonics of the Yb:YAG amplifier can be used to pump few-cycle pulses in visible or mid-infrared spectral range [16].

6. Outlook

The capabilities of the current high harmonic generation sources, based on CPA Ti:Sa technology, are limited to energies around a few hundred eV and to pulse durations of several tens of attoseconds. This limitation originates from a deficiency of the current laser technology that can either provide pulses with ultrahigh (petawatt) peak powers at relatively low repetition rates or moderate peak power (gigawatt) pulses at kHz repetition rates. Scaling attosecond pulses to high repetition rates and photon energies as high as several keV demands few-cycle laser systems with high peak and average power, which is beyond the performance of the current laser technology.

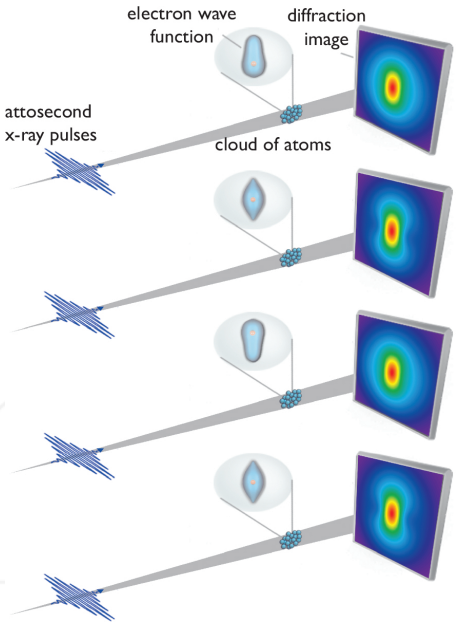

Figure 8. Attosecond X-ray diffraction: as a coherently induced charge oscillation takes place in an atom or molecule, an incident X-ray pulse takes a diffraction snapshot of the electron distribution at the time of interaction; changing the time delay between the source of the excitation and the attosecond pulse allows for the temporal evolution of the charge density to be directly measured in time and space. The figure represents the simulated dynamic of hydrogen atoms when they are exposed to 100-as, X-ray pulses and are excited into the 1S-2P coherent superposition state. As shown, the electron dynamic can be reconstructed by means of attosecond X-ray diffraction spectroscopy [3].

OPCPAs are scalable in terms of peak and average power and directly benefit from the availability of turn-key, industrial-grade ps-pump lasers. For more than two decades, powerful, cost-effective ps pump sources have been unavailable. Nowadays, diode-pumped ytterbium-doped lasers in the thin-disk geometry are able to deliver 1 ps scale pulses at kilowatt-scale average power, in combination with terawatt-scale peak powers. By merging these two existing technologies, and comprising OPCPAs driven by ytterbium-based pump lasers, the new generation of femtosecond technology will combine terawatt-scale peak powers with kilowatt-scale average powers in ultrashort optical pulse generation opening new path in the generation of isolated attosecond pulses with higher flux and photon energies.

The increased photon flux will greatly expand the applicability of attosecond spectroscopy to scrutinizing phenomena where current-generation sources delivered signal near or below the noise level, whereas shorter wavelengths provide direct access to electronic motions on increasingly shorter length scales from nanostructures toward atomic dimensions.

The availability of attosecond X-ray pulses could lead to resolve the spatiotemporal motion of electrons in their ultimate resolution, picometer-attosecond resolution, via attosecond X-ray diffraction spectroscopy (**Figure 8**).

Acknowledgements

I wish to thank Prof. Ferenc Krausz for fruitful discussions about the material of this chapter.

Author details

Hanieh Fattahi

Address all correspondence to: hanieh.fattahi@mpq.mpg.de

Max-Planck Institut für Quantenoptik, Garching, Germany and Department für Physik, Ludwig-Maximilians-Universität München, Garching, Germany

References

[1] H. Fattahi, H. G. Barros, M. Gorjan, T. Nubbemeyer, B. Alsaif, C. Y. Teisset, M. Schultze, S. Prinz, M. Haefner, M. Ueffing, A. Alismail, L. Vámos, A. Schwarz, O. Pronin, J. Brons, X. T. Geng, G. Arisholm, M. Ciappina, V. S. Yakovlev, D. E. Kim, A. M. Azzeer, N. Karpowicz, D. Sutter, Z. Major, T. Metzger, and F. Krausz, "Third-generation femtosecond technology," Optica 1, 45–63 (2014).

[2] M. Hentschel, R. Kienberger, C. Spielmann, G. A. Reider, N. Milosevic, T. Brabec, P. Corkum, U. Heinzmann, M. Drescher, and F. Krausz, "Attosecond metrology," Nature 414, 509–513 (2001).

[3] F. Krausz and M. Ivanov, "Attosecond physics," Rev. Mod. Phys. 81, 163–234 (2009).

[4] A. Dubietis, G. Jonušauskas, and A. Piskarskas, "Powerful femtosecond pulse generation by chirped and stretched pulse parametric amplification in BBO crystal," Opt. Commun. 88, 437–440 (1992).

[5] C. Le Blanc, P. Curley, and F. Salin, "Gain-narrowing and gain-shifting of ultra-short pulses in Ti: sapphire amplifiers," Opt. Commun. 131, 391–398 (1996).

[6] M. Lenzner, J. Krüger, S. Sartania, Z. Cheng, C. Spielmann, G. Mourou, W. Kautek, and F. Krausz, "Femtosecond optical breakdown in dielectrics," Phys. Rev. Lett. 80, 4076–4079 (1998).

[7] H. Fattahi, "Third-generation femtosecond technology," Springer Theses (Springer International Publishing, Cham, 2015).

[8] D. Herrmann, L. Veisz, R. Tautz, F. Tavella, K. Schmid, V. Pervak, and F. Krausz, "Generation of sub-three-cycle, 16 TW light pulses by using noncollinear optical parametric chirped-pulse amplification," Opt. Lett. 34, 2459–2461 (2009).

[9] N. Ishii, L. Turi, V. S. Yakovlev, T. Fuji, F. Krausz, A. Baltuska, R. Butkus, G. Veitas, V. Smilgevicius, R. Danielius, and A. Piskarskas, "Multimillijoule chirped parametric amplification of few-cycle pulses," Opt. Lett. 30, 567–569 (2005).

[10] M. Schultze, T. Binhammer, G. Palmer, M. Emons, T. Lang, and U. Morgner, "Multi-μJ, CEP-stabilized, two-cycle pulses from an OPCPA system with up to 500 kHz repetition rate," Opt. Express 18, 27291–27297 (2010).

[11] F. Röser, T. Eidam, J. Rothhardt, O. Schmidt, D. N. Schimpf, J. Limpert, and A. Tünnermann, "Millijoule pulse energy high repetition rate femtosecond fiber chirped-pulse amplification system," Opt. Lett. 32, 3495–3497 (2007).

[12] P. Russbueldt, T. Mans, G. Rotarius, J. Weitenberg, H. D. Hoffmann, and R. Poprawe, "400W Yb:YAG Innoslab fs-amplifier," Opt. Express 17, 12230–12245 (2009).

[13] L. E. Zapata, H. Lin, A.-L. Calendron, H. Cankaya, M. Hemmer, F. Reichert, W. R. Huang, E. Granados, K.-H. Hong, and F. X. Kärtner, "Cryogenic Yb:YAG composite-thin-disk for high energy and average power amplifiers," Opt. Lett. 40, 2610–2613 (2015).

[14] O. H. Heckl, J. Kleinbauer, D. Bauer, S. Weiler, T. Metzger, and D. H. Sutter, "Ultrafast Thin-Disk Lasers," 93–115 (2016) DOI: 10.1007/978-3-319-17659-8_5.

[15] H. Fattahi, A. Alismail, H. Wang, J. Brons, O. Pronin, T. Buberl, L. Vámos, G. Arisholm, A. M. Azzeer, and F. Krausz, "High-power, 1-ps, all-Yb:YAG thin-disk regenerative amplifier," Opt. Lett. 41, 1126–1129 (2016).

[16] Y. Deng, A. Schwarz, H. Fattahi, M. Ueffing, X. Gu, M. Ossiander, T. Metzger, V. Pervak, H. Ishizuki, T. Taira, T. Kobayashi, G. Marcus, F. Krausz, R. Kienberger, and N. Karpowicz, "Carrier-envelope-phase-stable, 1.2 mJ, 1.5 cycle laser pulses at 2.1 μm," Opt. Lett. 37, 4973–4975 (2012).

[17] D. Strickland and G. Mourou, "Compression of amplified chirped optical pulses," Opt. Commun. 55, 447–449 (1985).

[18] M. Guardalben, J. Keegan, L. Waxer, V. Bagnoud, I. Begishev, J. Puth, and J. Zuegel, "Design of a highly stable, high-conversion-efficiency, optical parametric chirped-pulse amplification system with good beam quality." Opt. Express 11, 2511–2524 (2003).

[19] L. J. Waxer, V. Bagnoud, I. A. Begishev, M. J. Guardalben, J. Puth, and J. D. Zuegel, "High-conversion-efficiency optical parametric chirped-pulse amplification system using spatiotemporally shaped pump pulses," Opt. Lett. 28, 1245–1247 (2003).

[20] L. Yu, X. Liang, L. Xu, W. Li, C. Peng, Z. Hu, C. Wang, X. Lu, Y. Chu, Z. Gan, X. Liu, Y. Liu, X. Wang, H. Lu, D. Yin, Y. Leng, R. Li, and Z. Xu, "Optimization for high-energy and high-efficiency broadband optical parametric chirped-pulse amplification in LBO near 800 nm," Opt. Lett. 40, 3412–3415 (2015).

[21] P. Wnuk, Y. Stepanenko, and C. Radzewicz, "Multi-terawatt chirped pulse optical parametric amplifier with a time-shear power amplification stage." Opt. Express 17, 15264–15273 (2009).

[22] J. Moses, C. Manzoni, S.-W. Huang, G. Cerullo, and F. X. Kaertner, "Temporal optimization of ultrabroadband high-energy OPCPA," Opt. Express 17, 5540–5555 (2009).

[23] G. Arisholm, "General numerical methods for simulating second-order nonlinear interactions in birefringent media," J. Opt. Soc. Am. B 14, 2543–2549 (1997).

[24] R. Szipocs, K. Ferencz, C. Spielmann, and F. Krausz, "Chirped multilayer coatings for broadband dispersion control in femtosecond lasers." Opt. Lett. 19, 201–203 (1994).

[25] T. Metzger, "High-repetition-rate picosecond pump laser based on a Yb:YAG disk amplifier for optical parametric amplification," PhD thesis (2009).

[26] C. Teisset, N. Ishii, T. Fuji, T. Metzger, S. Köhler, R. Holzwarth, A. Baltuska, A. Zheltikov, and F. Krausz, "Soliton-based pump-seed synchronization for few-cycle OPCPA." Opt. Express 13, 6550–6557 (2005).

[27] A. Schwarz, M. Ueffing, Y. Deng, X. Gu, H. Fattahi, T. Metzger, M. Ossiander, F. Krausz, and R. Kienberger, "Active stabilization for optically synchronized optical parametric chirped pulse amplification," Opt. Express 20, 5557–5565 (2012).

[28] S. Adachi, N. Ishii, T. Kanai, A. Kosuge, J. Itatani, Y. Kobayashi, D. Yoshitomi, K. Torizuka, and S. Watanabe, "5-fs, multi-mJ, CEP-locked parametric chirped-pulse amplifier pumped by a 450-nm source at 1 kHz," Opt. Express 16, 14341–14352 (2008).

[29] M. Puppin, Y. Deng, O. Prochnow, J. Ahrens, T. Binhammer, U. Morgner, M. Krenz, M. Wolf, and R. Ernstorfer, "500 kHz OPCPA delivering tunable sub-20 fs pulses with

15 W average power based on an all-ytterbium laser," Opt. Express 23, 1491–1497 (2015).

[30] J. Rothhardt, S. Demmler, S. Hädrich, J. Limpert, and A. Tünnermann, "Octave-spanning OPCPA system delivering CEP-stable few-cycle pulses and 22 W of average power at 1 MHz repetition rate," Opt. Express 20, 10870–10878 (2012).

[31] F. Tavella, Y. Nomura, L. Veisz, V. Pervak, A. Marcinkevius, and F. Krausz, "Dispersion management for a sub-10-fs, 10 TW optical parametric chirped-pulse amplifier," Opt. Lett. 32, 2227–2229 (2007).

[32] V. Pervak, I. Ahmad, M. K. Trubetskov, A. V. Tikhonravov, and F. Krausz, "Double-angle multilayer mirrors with smooth dispersion characteristics," Opt. Express 17, 7943–7495 (2009).

[33] D. Franz, H. Fattahi, V. Pervak, M. Trubetskov, E. Fedulova, N. Karpowicz, Z. Major, and F. Krausz, "Investigation of temporal compression of few-cycle pulses from an ultrabroadband, multi-mJ optical parametric amplifier," in "Conf. Lasers Electro-Optics—Int. Quantum Electron. Conf." (2013), p. CFIE_P_3.

[34] T. Buberl, A. Alismail, H. Wang, N. Karpowicz, and H. Fattahi, "Self-compressed, spectral broadening of a Yb:YAG thin-disk amplifier," Opt. Express 24, 10286–10294 (2016).

[35] W. Schweinberger, A. Sommer, E. Bothschafter, J. Li, F. Krausz, R. Kienberger, and M. Schultze, "Waveform-controlled near-single-cycle milli-joule laser pulses generate sub-10 nm extreme ultraviolet continua," Opt. Lett. 37, 3573–3755 (2012).

[36] Y. Deng and F. Krausz, "Method and device for optical parametric chirped pulse amplification," WO/2013/020671 PCT/EP2012/003283, 14.02.2013, 01.08.2012 (2013).